Available online at www.sciencedirect.com
SCIENCE DIRECT
Carbohydrate Polymers 57 (2004) 45–54
Carbohydrate Polymers
www.elsevier.com/locate/carbpol

Interfacial shear rheology of interacting carbohydrate polyelectrolytes at the water–oil interface using an adapted conventional rheometer

J.P. Pérez-Orozco[a,b], C.I. Beristain[c], G. Espinosa-Paredes[a], C. Lobato-Calleros[d], E.J. Vernon-Carter[a,*]

[a]*Departamento de Ingeniería de Procesos e Hidráulica, Universidad Autónoma Metropolitana-Iztapalapa, San Rafael Atlixco 186. C.P. 09340 México, D.F., Mexico*
[b]*Departamento de Ingeniería Química y Bioquímica, Instituto Tecnológico de Zacatepec, CP. 62780, Zacatepec, Mor., Mexico*
[c]*Instituto de Ciencia Básicas, Universidad Veracruzana, Apdo. Postal 575, Xalapa, Ver., Mexico*
[d]*Departemento de Preparatoria Agrícola, Universidad Autónoma Chapingo, C.P. 56230, Texcoco, Edo. Mex., Mexico*

Received 2 December 2003; revised 25 March 2004; accepted 30 March 2004

Abstract

A conventional rheometer was adapted for carrying out interfacial shear measurements. The interfacial shear viscosity and the interfacial creep compliance-time properties of mesquite gum or mesquite gum–chitosan mixed films were determined at the water–mineral oil interface. The ratio of chitosan to mesquite gum, and aging time, influenced the interfacial shear viscosity and interfacial creep compliance-time properties of the films. Electrostatic coulombic interactions arose between the negatively charged mesquite gum and the positively charged chitosan molecules, and the strength of the interaction was influenced by the relative charge density between both biopolymers.

The interfacial shear viscosity and the interfacial viscoelastic properties of films obtained from 10% (w/w) mesquite gum aqueous solutions were boosted by the addition of chitosan at concentrations of 0.2–0.6% (w/w), but depressed by addition of chitosan at concentrations of 0.8–1.0% (w/w).

Keywords: Interfacial shear viscosity; Interfacial creep compliance-time properties; Carbohydrate polyelectrolytes; Electrostatic interactions

1. Introduction

It is known that biopolymer complexes possess the capacity to form and stabilize dispersed food systems, and that such complexes are mainly formed between oppositely charged macromolecules (Plashchina et al., 2001), particularly between proteins and polysaccharides below their isoelectric point (Renard, Boué, & Lefebvre, 1997). Thermodynamic equilibrium between a protein–polysaccharide blend can be achieved when attractive interactions between the biopolymers is favored to the detriment of the solvent by the so-called complex coacervation phenomenon (Schmitt et al., 2001). Such is the case between casein and low-methoxyl pectin at low pH, where the binding of pectin to casein particles is the result of the interactions between the negative charges of the pectin and the positive charges of the casein below its isoelectric point, and where a surface of casein appears to be required for adsorption of pectin (Dalglish & Hollocou, 1997). There have been no studies of the interactions between polysaccharides charged oppositely, and in which one possesses surface activity and the other does not.

Mesquite gum (*Prosopis spp.*) has been proposed as substitute of gum arabic (*Acacia senegal*) and is reported as being an excellent encapsulating agent of essential oils over a wide range of water activities, and an emulsifying and stabilizing agent of natural colorants extending their shelf-life beyond that provided by gum arabic (Beristain, Azuara, & Vernon-Carter, 2002; Pérez-Alonso et al., 2003). The film forming ability of mesquite gum is due to formation of a macromolecular stabilizing layer around oil droplets, and not by modification of the aqueous phase rheology. Due to its rather low surface activity as compared to protein emulsifiers, fairly high gum-to-oil weight ratio is required for obtaining stable oil-in-water emulsions with

* Corresponding author. Tel.: +52-5804-4648; fax: +52-5724-4900.
E-mail address: jvc@xanum.uam.mx (E.J. Vernon-Carter).

0144-8617/$ - see front matter © 2004 Elsevier Ltd. All rights reserved.
doi:10.1016/j.carbpol.2004.03.022

small and homogeneous droplet size (Vernon-Carter, Pedroza-Islas, & Beristain, 2000).

Mesquite gum is a complex branched heteropolyelectrolyte with a backbone of 1,3-linked β-galactopyranose units and side chains of 1,6-linked galactopyranose units terminating in glucuronic acid or 4-*O*-methylglucuronic acid residues. Mesquite gum from *Prosopis laevigata* has been reported as containing a small amount of protein (2.7 ± 0.06%), covalently linked to the carbohydrate moieties. The gum is a complex mixture of at least four distinct fractions with different chemical structures. The protein element is mainly associated with a high molecular mass fraction representing less than 11% of the total gum (Orozco-Villafuerte, Cruz-Sosa, Ponce-Alquicira, & Vernon-Carter, 2003).

Chitosans are linear polysaccharides containing two sugar residues, *N*-acetyl-D-glucosamine and d-glucosamine, respectively, which are both β-1,4-linked. Chitosans are normally polydisperse, and have the ability to dissolve in dilute aqueous acidic solutions. Their molecular weight ranges from 10,000 to 1,000,000 g/mol. The polymer has the shape of an expanded random coil in solution (Fredheim & Christensen, 2003). Due to its cationic character, chitosan has received increasing attention as a polymer component of polyelectrolyte complexes, as it has the capability of forming films with good mechanical and permeability properties, and as a potential microencapsulation agent (Goycoolea, Argüelles-Monal, Peniche, & Higuera-Ciapara, 2000). Chitosan is increasingly being used to improve microbiological stability of products such as food emulsions, but its application in products in which emulsifying capacity is important for achieving processing efficiency (e.g. microencapsulation by spray-drying of essential oils) is limited, despite its good film forming properties.

Interfacial shear rheology of adsorbed biopolymer layers yields information about their structural state at the interface (Martin & van Vliet, 2001). Interfacial shear properties have a substantial influence in the dynamic processes at fluid interfaces and are relevant in technological problems like the formation, stability and rheology of emulsions and foams, and other film coating processes (Dickinson, 2003; Jones & Middelberg, 2002; Langevin, 2000; Petkov, Danov, & Denkov, 1996). It has been suggested that the creation of a gel like-adsorbed film provides high resistance against shear around an emulsion droplet, suppresses droplet deformation and breakup, and retards droplet coalescence (Martin, Bos, Cohen, & van Vliet, 2002).

The determination of interfacial shear properties, along with other interfacial properties, are useful as indicators of the structural state of adsorbed biopolymer layers at liquid-liquid and gas–liquid interfaces (Dickinson, 1999; Murray & Dickinson, 1996; Sánchez-González, Cabrerizo-Vílchiz, & Gálvez-Ruíz, 1999). The rheological characteristics of adsorbed biopolymer films as a function of film aging are a reflection of particularly restructuring phenomena that occur after molecular adsorption (Roth, Murray, & Dickinson, 2000). The interfacial shear rheology of adsorbed biopolymer appears to be sensitive to the detailed macromolecular structure and to the nature of the intermolecular interactions of the adsorbed layer (Murray, Dickinson, & Stainsby, 1985; Rodríguez-Patiño & Niño, 1999).

In literature various methods to determine shear properties of adsorbed layers have been described (Joly, 1972; Roth et al., 2000), among them the Couette type surface rheometers (Chen & Dickinson, 1995; Martin et al., 2002; Ogden & Rosenthal, 1997; Vernon-Carter & Sherman, 1981). The use of this type of rheometers allows the determination of the interfacial shear viscosity, and the interfacial viscoelastic properties of the adsorbed biopolymer films at fluid interfaces (Sherman, 1970).

In this work a conventional rheometer was adapted for determining the interfacial shear viscosity and interfacial viscoelastic properties of adsorbed films of oppositely charged polysaccharides (anionic mesquite gum and cationic chitosan) at the oil–water interface, formed with varying proportions of chitosan to mesquite gum, and at different aging times.

2. Materials and methods

2.1. Equipment

A Physica MCR 300 (Physica Meßtechnik GmbH, Stuttgart, Germany) modular compact rheometer was adapted for carrying out the interfacial shear measurements. The MCR 300 rheometer can work under controlled stress or controlled strain conditions. It has a torque measurement range of 0.02 μNm–150 mNm with a resolution of 0.002 μNm and angular resolution of less than 0.1 μrad. A stainless steel biconical disk was requested to be machined by Physica Meßtechnik, with the following physical dimensions: radius of disk, R_b, of 15 mm and disk double angle, 2α, of 10°, in order to achieve a perfect coupling with the rheometer motor drive and avoid eccentricity. A thermostated acrylic vessel was made at the Universidad Autonoma Metropolitana-Iztapalapa (Mexico City, Mexico) mechanical shop with an inner radius, R_c, of 27 mm. The acrylic vessel was then inserted in the measuring plate of the rheometer. Afterwards the rheometer motor drive was lowered so that the stainless steel biconical disk was placed at the polysaccharides blend aqueous surface. Then the oil phase was carefully poured with help of a glass rod unto the vertical wall of the vessel until the oil formed a layer above the polysaccharides blend solution. The age of the interface was taken from the moment the last drop of oil was poured in. Fig. 1 shows a photograph of the vessel and biconical disk mounted on the conventional rheometer, and a schematic diagram showing the setup of the system.

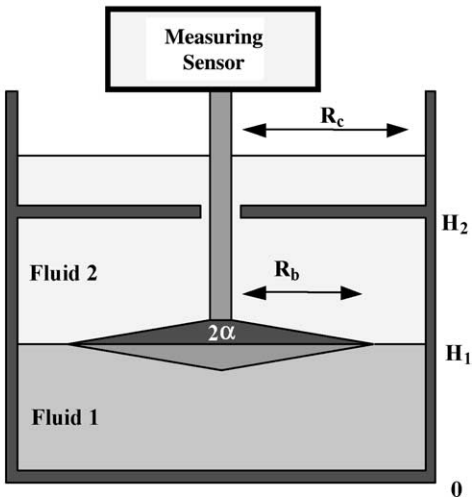

Fig. 1. Photograph showing the adaptations made to the conventional rheometer and schematic diagram showing the physical dimensions of the measuring system (biconical disk and containing vessel). R_b : radius of biconical disk, R_c : radius of vessel, α : half angle of biconical disk, H_1 : depth of fluid 1, H_2 : depth of fluid 2.

2.2. Calculations

The torque required for maintaining the dish moving at a constant angular velocity at the interface can be calculated with the following equation, when the force contributions of the upper and lower fluid phases are negligible compared to those of the interface:

$$M = 2\pi r \sigma^{\text{int}} r \tag{1}$$

where $2\pi r\sigma^{\text{int}}$ is the interfacial force, σ^{int} is the interfacial shear stress and r is the radial location between the disk and the vessel ($R_b \leq r \leq R_c$), as is illustrated in Fig. 1. Here M is the torque measured by the equipment.

The interfacial shear stress is a function of the radial coordinate, which can be obtained with Eq. (1) as follows:

$$\sigma^{\text{int}} = \frac{M}{2\pi r^2} \tag{2}$$

The interfacial shear rate for a rotational system is a function of angular velocity ω, as follows:

$$\frac{\mathrm{d}\gamma^{\text{int}}}{\mathrm{d}t} = -\frac{\mathrm{d}u}{\mathrm{d}r} = -r\frac{\mathrm{d}\omega}{\mathrm{d}r} \tag{3}$$

The interfacial shear rate can also be expressed as a function of the interfacial shear stress:

$$\frac{\mathrm{d}\gamma^{\text{int}}}{\mathrm{d}t} = f(\sigma^{\text{int}}) \tag{4}$$

According with Eq. (2) the radial variable is given by:

$$r = \left(\frac{M}{2\pi}\right)^{(1/2)} (\sigma^{\text{int}})^{-(1/2)} \tag{5}$$

Now, deriving this equation with respect σ^{int} and substituting Eq. (1), we have:

$$\frac{\mathrm{d}r}{\mathrm{d}\sigma^{\text{int}}} = -\frac{1}{2} r (\sigma^{\text{int}})^{-1} \tag{6}$$

where M is constant and

$$\frac{\mathrm{d}r}{r} = -\frac{1}{2}\frac{\mathrm{d}\sigma^{\text{int}}}{\sigma^{\text{int}}} \tag{7}$$

Substituting Eqs. (4) and (7) into Eq. (3), we find the following results:

$$\mathrm{d}\omega = \frac{1}{2} f(\sigma^{\text{int}}) \frac{\mathrm{d}\sigma^{\text{int}}}{\sigma^{\text{int}}} \tag{8}$$

This equation allows us to establish relationship of the angular velocity as a function of the interfacial shear stress. Integrating Eq. (8) between the inner radius of the disk R_b with $\omega = \Omega$ and the stationary outer vessel radius R_c with $\omega = 0$.

$$\int_{\omega=\Omega}^{\omega=0} \mathrm{d}\omega = \int_{\sigma_b^{\text{int}}}^{\sigma_c^{\text{int}}} f(\sigma^{\text{int}}) \frac{\mathrm{d}\sigma^{\text{int}}}{\sigma^{\text{int}}} \tag{9}$$

leading to

$$\Omega = -\frac{1}{2} \int_{\sigma_b^{\text{int}}}^{\sigma_c^{\text{int}}} f(\sigma^{\text{int}}) \frac{\mathrm{d}\sigma^{\text{int}}}{\sigma^{\text{int}}} \tag{10}$$

where σ_c^{int} and σ_b^{int} are the interfacial shear stress in the outer vessel radius and inner radius of the disk, respectively.

The right hand side of Eq. (10) can be solved if the following conditions are considered:

C.1 The interface is incompressible and Newtonian.
C.2 The velocity distribution and the form of the interface is independent of time.
C.3 The interface is flat and homogeneous.
C.4 Inertial effects are negligible compared to the viscous effects of the system.
C.5 The velocity of the fluid at the bottom, surface and walls is zero.

Applying C.1, C.2 and C.4 we can establish the functionality of the $f(\sigma^{int})$ as follows:

$$f(\sigma^{int}) = \frac{\sigma^{int}}{\eta^{int}} \tag{11}$$

Then, substituting this equation into Eq. (10) and considering the conditions C.2, C.3 and C.5, the integral results in:

$$\Omega = -\frac{1}{2}\int_{\sigma_b^{int}}^{\sigma_c^{int}} \frac{\sigma^{int}}{\eta^{int}} \frac{d\sigma^{int}}{\sigma^{int}} = -\frac{1}{2\eta^{int}}(\sigma_c^{int} - \sigma_b^{int}) \tag{12}$$

This equation allows the evaluation of the interfacial shear viscosity in terms of known parameters:

$$\eta^{int} = \frac{M}{4\pi\Omega}\left(\frac{1}{R_b^2} - \frac{1}{R_c^2}\right) \tag{13}$$

where

$$\sigma_c^{int} = M/(2\pi R_c^2) \tag{14}$$

and

$$\sigma_b^{int} = M/(2\pi R_b^2) \tag{15}$$

This equation is used for determining the interfacial shear viscosity.

For determining the strain at the interface at any time t we have that:

$$\frac{d\gamma^{int}}{dt} = \frac{\sigma_c^{int}}{\eta^{int}} \tag{16}$$

Integrating this equation between $t = 0$ with $\gamma^{int}(0) = 0$ and $t = t$ with $\gamma^{int}(t) = \gamma^{int}$, we obtain:

$$\gamma^{int} = \int_0^t \frac{\sigma_c^{int}}{\eta^{int}} dt = \frac{\sigma_c^{int}}{\eta^{int}} t \tag{17}$$

Substituting Eqs. (13) and (14) into Eq. (17), we obtain that the interfacial shear strain can be calculated in terms of known parameters and as a function of time:

$$\gamma^{int}(t) = \frac{2R_b^2}{(R_c^2 - R_b^2)}\Omega t \tag{18}$$

where Ωt corresponds to the angular displacement of the disk by an angle $\theta(t)$ as a function of time t, which is measurement by the rheometer. Eqs. (2), (13) and (18) are the classical equations reported in interfacial shear rheological studies (Chen & Dickinson, 1995; Martin et al., 2002; Murray et al., 1985; Ogden & Rosenthal, 1997; Vernon-Carter & Sherman, 1981).

2.3. Materials

Medium molecular weight chitosan was purchased from Sigma-Aldrich Quimica, S.A. de C.V. (Toluca, Mexico). Mesquite gum (MG) tears were hand collected in the Mexican state of San Luis Potosi, Mexico, and purified as reported by Vernon-Carter et al. (1996). Acetic acid was from J.T. Baker, S.A. de C.V. (Xalostoc, Mexico). White mineral oil was purchased from Drogueria Cosmopolitana, S.A. de C.V (Mexico City, Mexico). The water used for all the experiments was double distilled and had a surface tension of 72 ± 0.4 mN m^{-1} at 25 °C.

Hen egg-white lysozyme was obtained from Sigma-Aldrich Quimica, S.A. de C.V. (Toluca, Mexico). AnalaR-grade buffer salts, potassium dihydrogen orthophosphate and disodium hydrogen orthophosphate, were obtained from J.T. Baker, S.A. de C.V. (Xalostoc, Mexico).

2.4. Aqueous solutions

In order to determine the effect of adding increasing concentrations of C upon the interfacial rheological properties of pure MG, 10% (w/w) MG aqueous solutions were added 0.2, 0.4, 0.6, 0.8 and 1.0% (w/w) C dissolved in 1.0% (w/w) acetic acid. All the polysaccharides blends were thoroughly mixed and let to stand for 1 h at room temperature before being put into the thermostated vessel.

2.5. Formation of the water–oil interface

Thirty milliliter of each polysaccharides blend was put into the thermostated vessel (depth H_1 17 mm in Fig. 1), the biconical disk lowered to the water-air interface, and this was immediately followed by careful addition of 30 ml of mineral oil to the disk (depth H_2 17 mm in Fig. 1), to form an oil layer above the polysaccharides blend solution.

2.6. Measurements

2.6.1. Data comparison

In order to determine if our adapted rheometer provided comparable results to those reported in the literature, the interfacial shear viscosity as a function of time of an aqueous solution of lysozyme (1×10^{-3}%, w/v, pH 7, 0.05 M, 20 °C) in contact with *n*-tetradecane was determined. These results were compared with those obtained by Ogden and Rosenthal (1997).

2.6.2. The interfacial shear viscosity

For the viscosity measurements, the film was subjected to a constant disk angular velocity (Ω) of 1.27×10^{-3} rad/s. The necessary torque (M) required for maintaining the steady rotational speed of the disk, and the resulting angular displacement of the disk with time $\theta_b(t)$ were monitored every 10 s for 15 min with the rheometer software. With the data σ^{int} and γ^{int} were calculated with Eqs. (2) and (18), and plots of σ^{int} versus γ^{int} were obtained in order to determine the region in which the torque and/or interfacial stress at the interface attains steady-state behavior, which was used in the calculation of η^{int} with Eq. (13). η^{int} was determined at different aging times of the films. All measurements were done at 25 °C.

2.6.3. Interfacial viscoelastic shear rheology

The interfacial creep compliance-time study of the interfacial films was carried out by applying a constant σ^{int} of 0.3535 mN m^{-1} during 15 min, after which σ^{int} was withdrawn, and the stress relaxation of the film was followed for further 15 min. The change in $\theta_b(t)$ was monitored every 2 s with the rheometer software and γ^{int} as a function of time was calculated with Eq. (18). The interfacial compliance of the films as a function of time was obtained with the following equation:

$$J(t) = \frac{\gamma^{int}(t)}{\sigma^{int}} \tag{19}$$

A plot of $J(t)$ versus t for each film was obtained. Interfacial creep compliance–time studies were carried out on the films aged 8, 16, 24, 36 and 48 h. The experimental data were non-linearly adjusted to the following equation (Sherman, 1968) using a Polymath software release 5.0 (Cache Corporation, Austin, TX, USA):

$$J(t) = J_0 + J_m(1 - e^{-(t/\lambda_m)}) + J_N \tag{20}$$

where J_0 ($= 1/E_0$; E_0 is the interfacial instantaneous elastic modulus) is the instantaneous interfacial elastic compliance in which bonds between the primary structural units are stretched elastically; J_m ($= 1/E_R$; E_R is the interfacial retarded elastic modulus) is the interfacial mean retarded compliance of all the bonds involved, λ_m ($= J_m/\eta_m$; η_m is the interfacial mean viscosity associated with retarded elasticity) is the interfacial mean retardation time, and J_N ($= t/\eta_N$) is the interfacial Newtonian compliance, which is characterized by an interfacial Newtonian viscosity η_N. All measurements were carried out at 25 °C.

2.7. Statistical analysis

An analysis of variance (ANOVA) and Tukey's test ($\alpha \leq 0.05$) was performed on interfacial creep compliance–time data of the films using the Statgraphics plus statistical analysis system (Statistical Graphics Corp. Manugistics Inc., Rockville, MD, USA).

3. Results and discussion

3.1. Data comparison

Comparison of the η^{int} versus aging time results of lysozyme obtained by us and that reported by Ogden and Rosenthal (1997) indicated that both curves exhibited the same tendency, with η^{int} showing an increase with aging time. Moreover, η^{int} exhibited by both curves was of the same order at all aging times (Fig. 2). Further data comparison beyond this point is difficult to establish, as there is no standardization of method. The equipments were made of different materials and dimensions, and perhaps more important, in this work the biconical disk was rotated at a known angular velocity, whereas in Ogden and Rosenthal's arrangement the vessel was rotated at a constant speed.

3.2. The interfacial shear viscosity

Fig. 3 shows a representative plot of σ^{int} versus γ^{int} for the interfacial film at the water–mineral oil interface arising from the 10% MG–0.6% C aqueous solution, at different aging times. These curves showed the same tendency as those for β-lactoglobulin and ovalbumin reported by Martin et al. (2002). The stress–strain curves aged 4 h or longer exhibited four distinct regions: (1) an initial region characterized by a steep increase in stress, (2) a stress maximum, (3) a steep decrease in stress, and (4) a steady-state or equilibrium shear stress region. Martin et al. (2002) mentioned that the maximum represents the maximum strength of the interfacial film and that it is related to its elastic properties, whereas the steady-state stress value is seen as the equilibrium shear stress in stationary flow characterizing the viscous properties of the interfacial film. The film aged 1 h deviated from this behavior probably because not enough time was allowed for adsorption of the biopolymers to take place at the interface, with only the viscous flow region being evident. As the films were aged for longer times the adsorbed biopolymer molecules underwent conformational rearrangements at the interface that led to the formation of more cohesive films via intermolecular interactions, so that σ^{int} required for achieving a given γ^{int} increased as film aging time increased. At low γ^{int} the bonds between the interacting biopolymers making up the interfacial film were stretched-out so that the linear stress–strain region extended up to ~3%. The maximum reached in the stress–strain curves (that increased as aging time of films increased) occurred at γ^{int} of about 4%, and represents the ultimate strength of the interfacial layer. The decrease in σ^{int} indicated that the interfacial film network suffered ongoing structure breakdown after failure. This region extended to strains up to 40%. The decrease in stress continued until equilibrium between the breaking and reformation of bonds took place, reaching the steady-state stress region. The interfacial shear viscosity was calculated with steady-state stress region

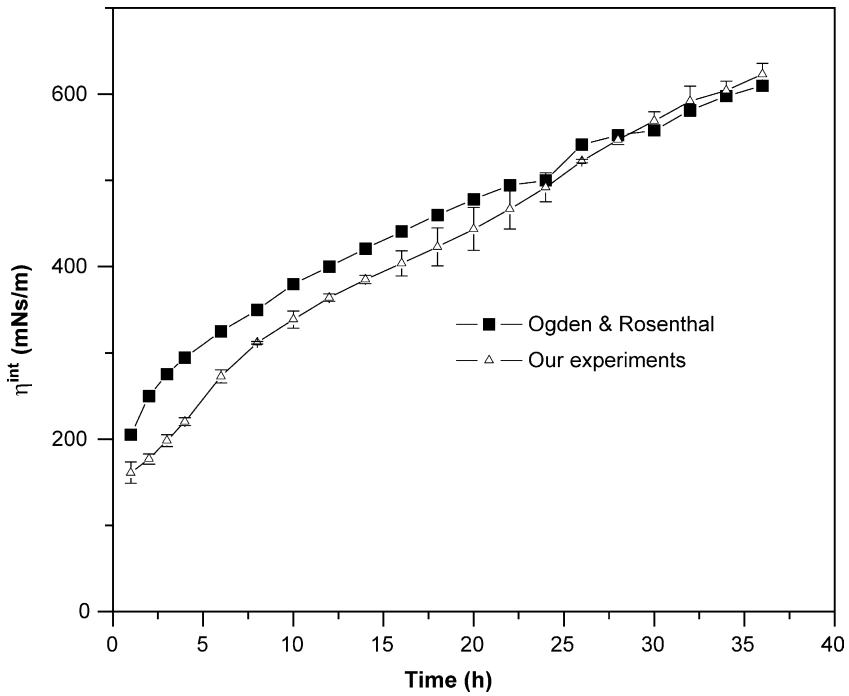

Fig. 2. Comparison between the data of the apparent surface shear viscosity with aging time of lysozyme obtained in this study and that by Ogden and Rosenthal (1997).

values. In the case films aged 1 h, η^{int} was calculated with the average value of the last 20 points for σ^{int} in the σ^{int} versus γ^{int} plot. The behavior depicted in Fig. 3 was followed by all the films studied.

Fig. 4 shows that all the different film formulations experienced an increase in η^{int} with aging time, and achieved structural equilibrium after about 16 h. The different η^{int} values with aging time indicate that the interactions arising between the two polyelectrolytes (MG and C) depend on their relative concentrations. Thus, the increase in η^{int} by films 10% MG–0.2% C, 10% MG–0.4% C, and 10% MG–0.6% C with regard to that of the pure mesquite gum film, pinpoints to complex formations arising due to the coulombic interactions

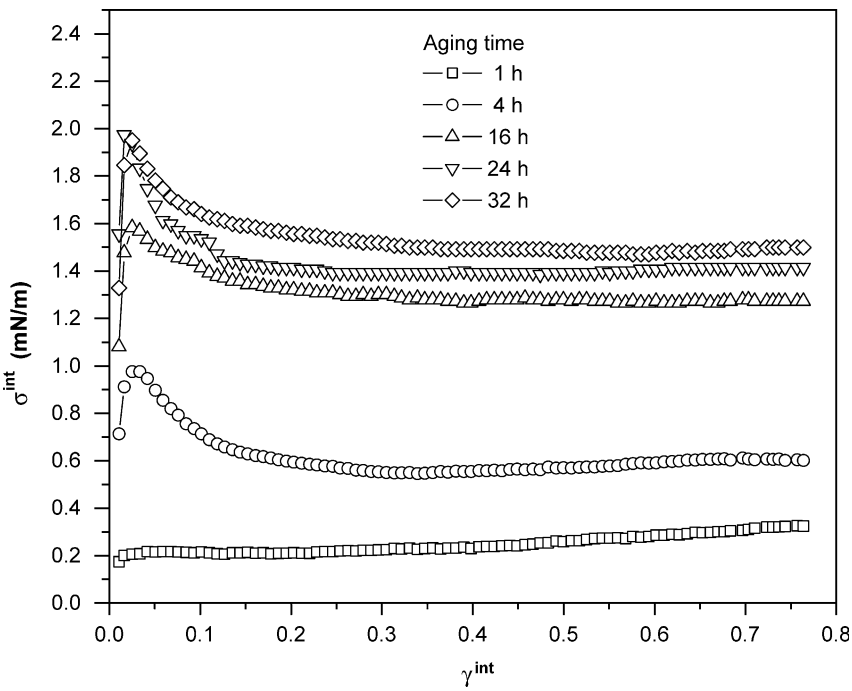

Fig. 3. Shear stress–strain relationship for film10% GM–0.6% C at different aging times.

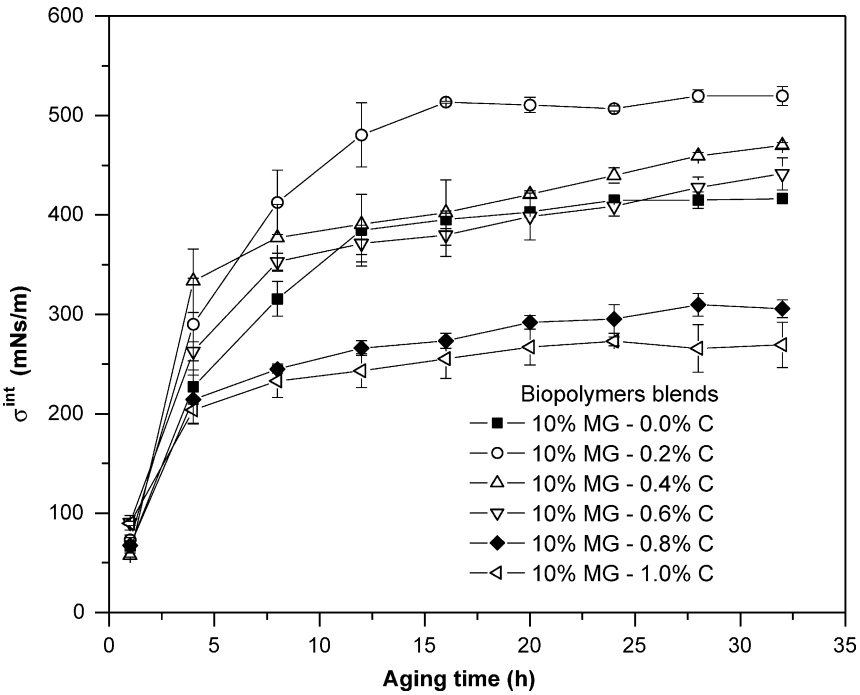

Fig. 4. Changes in the interfacial shear viscosity with aging time of films.

between the positively charged chitosan molecules and the negatively charged molecules of mesquite gum. At the pH (~3.8) of the biopolymers blends aqueous solutions it would seem that mesquite gum molecules have a relatively moderate to low negative charge density, while the chitosan molecules have a relatively high positive charge density. At 0.2% C the positive charge density of C seems to be equilibrated with the negative charge density of MG, and a strong electrostatic interaction arises between both molecules producing a synergetic increase in η^{int} of the film as multilayer structures are formed at the water–oil interface. However as the concentration of C increases to 0.4 and 0.6% in the blends, the positive charge density of C is larger than the negatively charge density of the MG molecules. While still both polyelectrolytes molecules tend to form electrostatic complexes, the increasingly higher positive charge density of the C molecules tend to shield the negatively charged ionized groups of MG, effectively lowering the attractive interaction between both molecules. The overall effect is that with increasing C concentration η^{int} of the films drops to approximately that of the pure MG film. As concentration of C is further increased to 0.8 and 1.0%, a great differential between C positive charges and MG negative charges arises, so that most of the ionizable groups of MG are shielded, shunning electrostatic interactions between both molecules. As a consequence of this, MG molecules tend to contract, so that a segregate phase separation between the C and MG molecules occurs in the bulk of the aqueous phase. Diffusion to and adsorption of the MG molecules to the interface takes place, but in their contracted form the intermolecular interactions between MG molecules are minimized, so that η^{int} of the films decreases. The higher the concentration of C in the aqueous bulk phase, the more compact the configuration of MG molecules at the interface, less MG-C interacting molecules are adsorbed at the interface, and the lower η^{int} of the films.

3.3. Creep compliance–time studies

All of the films aged 24 h showed typical interfacial creep compliance–time curves (Fig. 5) (curves for 0.8 and 1% w/w C are not shown they fell out of range) indicating that all exhibited viscoelastic behavior, which was affected by the addition of different concentrations of C to MG. The viscoelastic parameters characterizing each film are given in Table 1. Analysis of the instantaneous interfacial compliance modulus (J_0) indicates that the addition of C in concentrations between 0.2 and 0.6% (w/w) to MG produced a significant increase in the value of E_0 of the films, achieving a peak value at 0.4% (w/w) C, but significantly lower E_0 values were exhibited as the concentration of C added to MG was increased to 0.8 and 1% (w/w). This behavior confirms that the nature of the intermolecular interactions at the interface between MG and C are profoundly influenced by their relative concentrations. The results of E_0 confirm the tendency shown in the interfacial shear viscosity results (Fig. 4) in that a maximum interaction and a segregate phase separation occurred at specific MG-C relative concentrations. Although the maximum in the interfacial shear viscosity occurred at 0.2% (w/w) C and that of E_0 at 0.4% (w/w) C these differences may be attributed to the nature of the rheological test involved. The interfacial creep compliance–time study is a non-destructive test, and permits the determination of

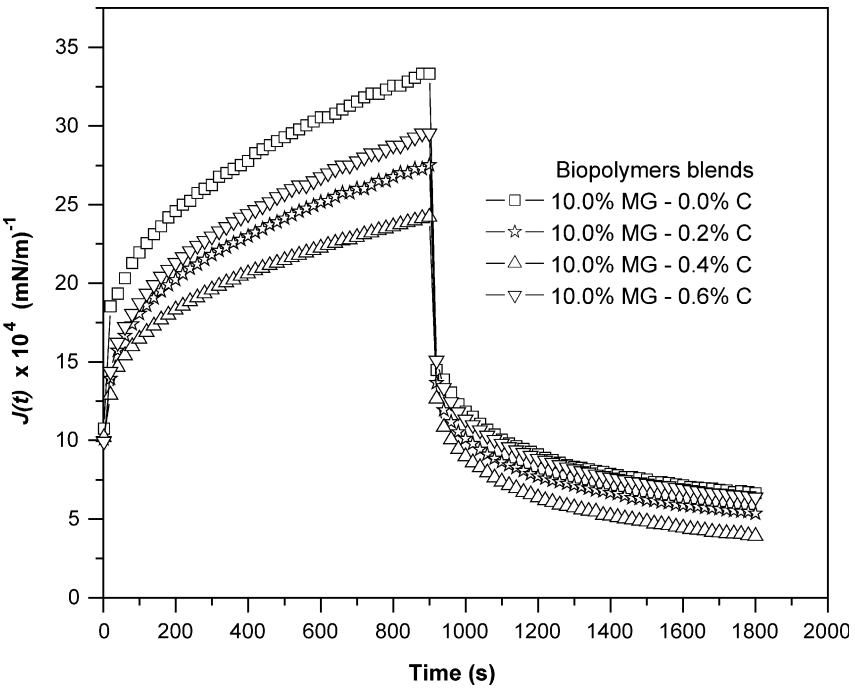

Fig. 5. Creep compliance–time curves for films with different concentrations of C.

rheological parameters under conditions that approach the state of the sample at rest, from which a more precise picture of the actual structure of the film may be drawn (Muñoz & Sherman, 1990). The retarded interfacial elastic compliance region parameters J_m and λ_m were also affected significantly by the concentration level of C added to MG. The values of J_m followed the same tendency than those exhibited by J_0 (i.e. showed a maximum at 0.4% (w/w) C), λ_m showed a more complex behavior. Also η_N was affected significantly by the amount of C added to MG, showing a maximum at 0.4% (w/w) C. The creep compliance–time behavior of the films corroborates the assumptions made by Martin et al. (2002) about the mechanisms giving rise to the four regions in the stress–strain curves depicted in Fig. 3. Thus the increase in the stress–strain curves can be related to E_0 which provides a measure of elastic strength of the bonds making up the interfacial network structure. The decrease in stress–strain curves can be associated to λ_m which gives a measure of the complexity of the type and diversity of the bonds in the structure (Lobato-Calleros, Aguirre-Mandujano, Vernon-Carter, & Sánchez-García, 2000). As stated above, the relative concentration of the positively and negatively charges affect the degree of interaction and induce conformational changes in the biopolymers, influencing the rate at which bonds are broken and reformed. All bonds do not break and reform at the same rate, however, the weaker bonds break at smaller values of t than the stronger ones giving place to different values of J_m and η_m (remembering that $\lambda_m = J_m/\eta_m$) once the instantaneous interfacial elastic modulus value is exceeded. The steady-state stress region characterized by η_N arises because following the rupture of some of the bonds, the time required for them to reform is longer than the test period, so that the broken bonds released structure units flow past one another (Sherman, 1970). Finally, the maximum occurring in the stress–strain curve corresponds to the point in the creep compliance–time curve where the threshold of the instantaneous elastic compliance is just exceeded and the onset of the interfacial elastic retarded compliance commences.

All of the films showed a change in their interfacial creep compliance with aging time. Fig. 6 illustrates this behavior

Table 1
Viscoelastic parameters for films made up with 10% (w/w) mesquite gum (MG) added with different concentrations of chitosan (C)

Biopolymers Blends	$J_0 \times 10^4$ (mN/m)$^{-1}$	$J_m \times 10^4$ (mN/m)$^{-1}$	t_m (s)	$\eta_N \times 10^4$ (mN s/m)
10.0%MG–0.0%C	14.06 ± 0.03^{c}	10.03 ± 0.82^{c}	78.53 ± 0.29^{b,c}	85.76 ± 4.95^{b}
10.0%MG–0.2%C	12.41 ± 0.04^{b}	7.13 ± 0.07^{a,b}	89.13 ± 5.83^{c}	106.03 ± 4.21^{d}
10.0%MG–0.4%C	10.17 ± 0.35^{a}	5.81 ± 0.16^{a}	51.325 ± 2.62^{a}	134.76 ± 0.96^{e}
10.0%MG–0.6%C	12.40 ± 0.41^{b}	8.25 ± 0.29^{b}	101.15 ± 7.76^{d}	98.63 ± 4.18^{c}
10.0%MG–0.8%C	16.22 ± 0.19^{d}	23.95 ± 0.31^{d}	68.61 ± 3.89^{b}	13.61 ± 0.08^{a}
10.0%MG–1.0%C	24.62 ± 0.70^{e}	33.73 ± 1.48^{e}	66.87 ± 2.1^{b}	9.45 ± 0.35^{a}

Data are means of three replicates per treatment.

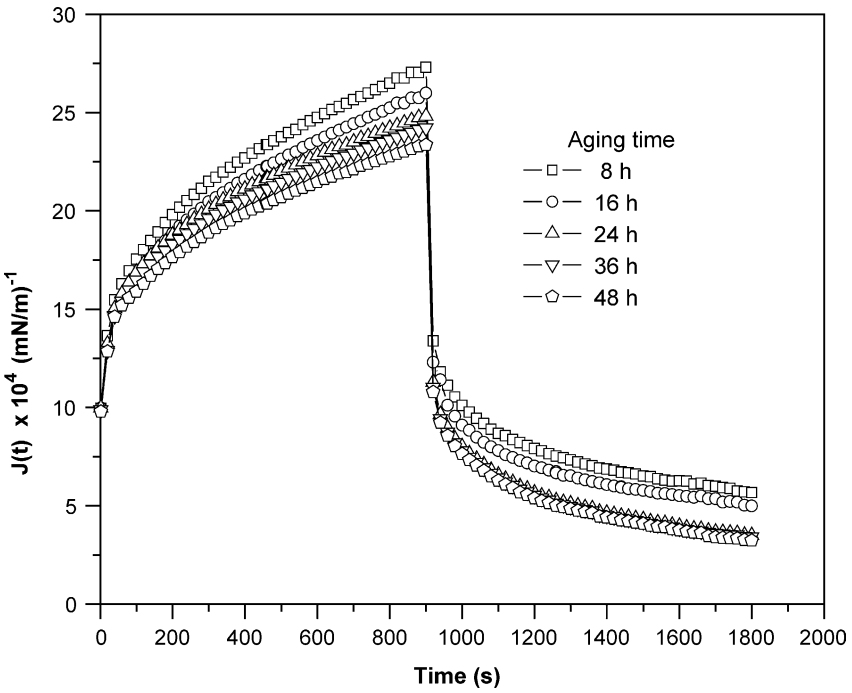

Fig. 6. Creep compliance–time curves for film 10% MG–0.4% C at different aging times.

for the 10% MG–0.4% C film, and the values of the interfacial viscoelastic parameters are given in Table 2. As can be seen the value of J_0 decreases steadily with aging time. These results indicated that ongoing rearrangements and intermolecular interactions took place between MG and C molecules at the interface and between the dangling moieties in the aqueous phase with aging time, increasing the structural strength of the film network. The decrease in J_0 with aging time was more pronounced as the initial value of J_0 was smaller, i.e. when interactions between the two biopolymers were stronger.

4. Conclusions

The physical adaptations made to the conventional rheometer and the application of interfacial theory allowed the measurement of the interfacial shear rheology properties and provided us with a clearer understanding regarding the mechanisms leading to the formation of the interfacial films.

The relative concentrations of MG and C affected the nature of the interactions between both molecules, and influenced the rheological properties of the adsorbed films. When the oppositely positive and negative charges of the biopolymers were balanced a strong electrostatic interaction arose giving place to the formation of strong viscoelastic coherent films, whose viscoelastic behavior increased with aging time. An excess in the density charge of the cationic polyelectrolyte relative to that of the anionic polyelectrolyte, promoted segregation processes between both molecules. The higher charge density of C affected the conformation of MG in bulk solution and at the interface, causing the MG to form weaker viscoelastic films, than those formed in the absence of C, or those in which the charge density of C was more balanced with that of MG. The interface creep compliance–time studies give a more

Table 2
Viscoelastic parameters for film 10% GM–0.4% C at different aging times

Aging time (h)	$J_0 \times 10^4$ (mN/m)$^{-1}$	$J_m \times 10^4$ (mN/m)$^{-1}$	λ_m (s)	$\eta_N \times 10^4$ (mNs/m)
8	11.62 ± 0.30^{b}	7.00 ± 0.21^{b}	91.53 ± 0.47^{b}	108.58 ± 3.75^{a}
16	11.441 ± 0.09^{b}	6.44 ± 0.40^{a,b}	84.00 ± 4.37^{b}	132.78 ± 2.36^{b}
24	10.17 ± 0.35^{a}	5.81 ± 0.16^{a}	51.325 ± 2.62^{a}	134.76 ± 0.96^{b}
36	9.97 ± 0.12^{a}	6.36 ± 0.65^{a,b}	53.94 ± 3.91^{a}	138.92 ± 4.66^{b,c}
48	9.72 ± 0.12^{a}	6.17 ± 0.11^{a,b}	56.54 ± 3.17^{a}	144.91 ± 3.11^{c}

Data are means of three replicates per treatment.

reliable idea of the structural features of the adsorbed films than the interfacial shear viscosity.

Acknowledgements

The authors are grateful for the financial support of this research from the Consejo Nacional de Ciencia y Tecnología (CONACyT) through grant G-33565-B, and to Ing. Rubén Ortega for his advice.

References

Beristain, C. I., Azuara, E., & Vernon-Carter, E. J. (2002). Effect of water activity on the stability to oxidation of spray-dried encapsulated orange peel oil using mesquite gum (*Prosopis juliflora*) as wall material. *Journal of Food Science*, *67*, 206–211.

Chen, J., & Dickinson, E. (1995). Surface shear viscosity and protein–surfactant interactions in mixed protein films adsorbed at the oil–water interface. *Food Hydrocolloids*, *9*, 35–42.

Dalglish, D. G., & Hollocou, A. L. (1997). Stabilization of protein-based emulsions by means of interacting polysaccharides. In E. Dickinson, & B. Bergenståhl (Eds.), *Foods colloids proteins, lipids and polysaccharides* (pp. 236–244). Cambridge: The Royal Society of Chemistry.

Dickinson, E. (1999). Adsorbed protein layers at fluid interfaces: interactions, structure and surface rheology. *Colloids and Surfaces B: Biointerfaces*, *15*, 161–176.

Dickinson, E. (2003). Hydrocolloids at interfaces and the influence on the properties of dispersed systems. *Food Hydrocolloids*, *17*, 25–39.

Fredheim, G. E., & Christensen, B. E. (2003). Polyelectrolyte complexes: Interactions between lignosulfonate and chitosan. *Biomacromolecules*, *4*, 232–239.

Goycoolea, F. M., Argüelles-Monal, W., Peniche, C., & Higuera-Ciapara, I. (2000). Chitin and chitosan. In G. Doxastakis, & V. Kiosseoglou (Eds.), *Novel macromolecules in food systems* (pp. 265–308). Amsterdam: Elsevier.

Joly, (1972). Rheological properties of monomolecular folms. Part I: basic concepts and experimental methods. In E. Matijevic (Ed.), (pp. 1–78). *Surface and Colloid Science*, New York: Wiley.

Jones, D. B., & Middelberg, A. (2002). Dierect determination of the mechanical properties of an interfacially adsorbed protein film. *Chemical Engineering Science*, *57*, 1711–1722.

Langevin, D. (2000). Influence of interfacial rheology on foam and emulsion properties. *Advances in Colloid and Interface Science*, *88*, 209–222.

Lobato-Calleros, C., Aguirre-Mandujano, E., Vernon-Carter, E. J., & Sánchez-García, J. (2000). Viscoelastic properties of white fresh cheese filled with sodium caseinate. *Journal of Texture Studies*, *31*, 379–390.

Martin, A., Bos, M., Cohen, M. S., & van Vliet, T. (2002). Stress–strain curves of adsorbed Protein layers at the air/water interface measured with surface shear rheology. *Langmuir*, *18*, 1238–1243.

Martin, A., & van Vliet, T. (2001). Interfacial rheological properties of adsorbed protein layers and surfactants: a review. *Advances in Colloid and Interface Science*, *91*, 437–471.

Muñoz, J., & Sherman, P. (1990). Dynamic viscoelastic properties of some commercial salad dressings. *Journal of Texture Studies*, *21*, 411–426.

Murray, B., Dickinson, E., & Stainsby, G. (1985). Time-dependent surface viscosity of adsorbed films of casein + gelatin at the oil–water interface. *Journal of Colloid and Interface Science*, *106*, 259–262.

Murray, B., & Dickinson, E. (1996). Interfacial rheology and the dynamic properties of adsorbed films of food proteins and surfactants. *Food Science and Technology International*, *2–3*, 131–145.

Ogden, L. G., & Rosenthal, A. J. (1997). Interactions between tristearin crystals and proteins at the oil–water interface. *Journal of Colloid and Interface Science*, *191*, 38–47.

Orozco-Villafuerte, J., Cruz-Sosa, F., Ponce-Alquicira, E., & Vernon-Carter, E. J. (2003). Mesquite gum: fractionation and characterization of the gum exuded from *Prosopis laevigata* obtained from plant tissue culture and wild trees. *Carbohydrate Polymers*, *54*, 323–327.

Plashchina, I. G., Mrachkovskaya, T. A., Danilenko, A. N., Kozhevnikov, G. O., Starodubrovskaya, N., Yu, ., Braudo, E. E., & Schwenke, K. D. (2001). Complex formation of faba bean legumin with chitosan: surface activity and emulsion properties complexes. In E. Dickinson, & R. Miller (Eds.), *Food colloid fundamentals of formulations* (pp. 293–303). Cambridge: The Royal Society of Chemistry.

Pérez-Alonso, C., Baéz-González, J. G., Beristain, C. I., Vernon-Carter, E. J., & Vizcarra-Mendoza, M. G. (2003). Estimation of the activation energy of carbohydrate polymers blends as selection criteria for their use as wall material for spray-dried microcapsules. *Food Carbohydrates*, *53*, 197–203.

Petkov, T., Danov, K. D., & Denkov, N. D. (1996). Precise method for measuring the shear surface viscosity of surfactant monolayers. *Langmuir*, *12*, 2650–2653.

Renard, D., Boué, F., & Lefebvre, J. (1997). Protein–polysaccharide mixtures: structure and effect of shear studied by small-angle neutron scattering. In E. Dickinson, & B. Bergenståhl (Eds.), *Foods colloids: proteins, lipids and polysaccharides* (pp. 305–315). Cambridge: The Royal Society of Chemistry.

RodríguezPatiño, J. M., & Niño, M. R. (1999). Interfacial characteristics of food emulsifiers (proteins and lipids) at the air-water interface. *Colloid and Surface B: Biointerfaces*, *15*, 235–252.

Roth, S., Murray, B. S., & Dickinson, E. (2000). Interfacial shear rheology of aged and heat-treated β-lactoglobulin films: displacement by nonionic surfactant. *Journal of Agricultural and Food Chemistry*, *48*, 1491–1497.

Sánchez-González, J., Cabrerizo-Vílchez, M. A., & Gálvez-Ruíz, M. J. (1999). Evaluation of the interactions between lipids and γ-globulin protein at the air–liquid interface. *Colloids and Surfaces B: Biointerfaces*, *12*, 123–138.

Schmitt, C., Sanchez, C., Despond, S., Renard, D., Robert, P., & Hardy, J. (2001). Structural modification of β-lactoglobulin as induced by complex coacervation with *Acacia* gum. In E. Dickinson, B. Dickinson, & B. Bergenståhl (Eds.), *Foods colloids: proteins, lipids and polysaccharides* (pp. 323–331). Cambridge: The Royal Society of Chemistry.

Sherman, P. (1968). Rheology of emulsions. In P. Sherman (Ed.), *Emulsion science* (pp. 217–247). London: Academic Press.

Sherman, P (1970). The relationship of shear and stress to textural properties of food. *Proceedings of the third International Congress of Food Science and Technology* (pp. 421-436). August 9–14, Washington, DC.

Vernon-Carter, E. J., Pedroza-Islas, R., & Beristain, C. I. (2000). Mesquite gum (*Prosopis* gum). In G. Doxastakis, & V. Kiosseoglou (Eds.), *Novel macromolecules in food systems* (pp. 217–238). Amsterdam: Elsevier.

Vernon-Carter, E. J., & Sherman, P. (1981). Rheological properties and applications of mesquite tree (*Prosopis juliflora*) gum. 4. Rheological properties of mesquite films at the oil–water interface. *Journal of Dispersion Science and Technology*, *2*, 399–414.

Vernon-Carter, E. J., Gómez, S. A., Beristain, C. I., Mosqueira, G., Pedroza-Islas, R., & Moreno-Terrazas, R. C. (1996). Color degradation and coalescence kinetics of aztec marigold oleoresin-in-water emulsions stabilized by mesquite or arabic gums and their blends. *Journal of Texture Studies*, *27*, 625–641.